Combined evaporator and condenser for sorption cooling systems: A steady-state performance analysis

G. Bamorovat Abadi, Majid Bahrami[*]

Laboratory for Alternative Energy Conversion (LAEC), School of Mechatronic Systems Engineering, Simon Fraser University, BC, V3T 0A3, Canada

A B S T R A C T

The main obstacles that prevent wide commercialization of sorption cooling/heat pump systems are their bulky size (weight), cost, and low efficiency. Combining two main cycle components, namely, evaporator and condenser, is a potential solution that can reduce the complexity, mass, and cost of such systems. Capillary-assisted low-pressure evaporators (CALPEs) are used in closed-cycle sorption systems including heat pumps, heat transformers, desalination, and thermal energy storage systems. This paper investigates the feasibility of a combined evaporator and condenser (CEC). A custom-built testbed for evaluating performance of CEC is used to test four types of commercially available finned-tube heat exchangers with a range of fin geometries. Tests were performed with water vapor pressure of 0.61 −5.63 kPa and 0−35 °C heat transfer fluid (HTF) inlet temperature. Comparing tubes with different fins indicates that tubes with 1.42 mm parallel fins, 40 fins per inch (FPI), have a higher overall heat transfer coefficient as an evaporator (40 W/K) and those with 0.9 mm cross head fins (40 FPI) marginally outperformed the other tubes as a condenser (47 W/K). Therefore, the capacity of the custom-built CEC is reported within practical operating temperature range.

© 2020 Elsevier Ltd. All rights reserved.

1. Introduction

The air conditioning & refrigeration (AC-R) industry is dominated by vapor compression refrigeration (VCR) technology that is driven by electricity, which is produced mainly from burning fossil fuel. Approximately 15% of the electricity produced globally is used by AC-R units [1−3]. A significant portion of the global greenhouse gas emission (GHG) is directly linked to this energy consumption and AC-R units. Sorption cooling systems (SCS) is alternative technology that can utilize waste heat (sources with temperatures around 80 °C), that is readily available from internal combustion engines, fuel cells, or other sources such as solar thermal panels, to produce cooling power. SCS is comprised of a sorption bed, an evaporator, and a condenser, assembled inside sealed chambers [4]. SCS have no harmful materials, no moving parts, and need negligible electrical power compared to VCR. It also eliminates the need for hydrofluorocarbons and provides a platform, as water can be used as the refrigerant, further addressing the climate change and promoting the phase-out of hydrofluorocarbons (HFC) [5].

However, commercialization of SCS faces major challenges, including i) low operating pressure, as saturated pressure for water at 5−20 °C is between 0.87 and 2.34 kPa [6], leading to major sealing and associated maintenance and cost issues; ii) low specific cooling power (SCP), due to poor heat (and/or mass) transfer in sorption beds; iii) low performance of currently available low-pressure evaporators; and iv) low coefficient of performance (COP) compared to VCR, in part due to high thermal inertia of the sorption beds and HEXs currently used in SCS. These, in turn, make the current SCS bulky and heavy, unreliable, and expensive. To address these issues, heat/mass exchangers need to be specifically designed and optimized for SCS. A potential solution to address these issues is to use a combined evaporator and condenser (CEC) to reduce weight, complexity, and cost.

Capillary-assisted low-pressure evaporators, CALPE, have been suggested and used in SCS. A CALPE eliminates the need for a circulating pump in the low-pressure evaporator taking advantage of the capillary effect. There are several experimental, numerical, and analytical studies published in the literature on the topic. Sabir et al. [7], presented their experimental results on the effect of a porous layer on the thermal performance of their water evaporators. They proposed an analytical model and reported good agreement between their model and experimental findings in

<div style="border:1px solid">

Nomenclature

A	heat transfer surface area (m^2)
c_p	heat capacity at constant pressure ($J/kg.K$)
D, d	diameter (m)
h	heat transfer coefficient ($W/(m^2 \cdot K)$)
k	thermal conductivity ($W/(m \cdot K)$)
L	heat transfer length of the evaporator tube (m)
$\dot{m}$	mass flow rate (kg/s)
p	pressure (Pa)
$\dot{Q}$	total heat transfer rate (W)
$\dot{q}$	heat transfer rate (W)
r	radius (m)
T	temperature ($^\circ C$)
T_i	inlet temperature ($^\circ C$)
T_o	outlet temperature ($^\circ C$)

T_{sat}	saturation temperature ($^\circ C$)
t	time (s)
t_1	start of steady state period (s)
t_2	end of steady state period (s)
Δt	time span of steady stated period (s)
ΔT_{LMTD}	logarithmic mean temperature difference ($^\circ C$)
U	overall heat transfer coefficient ($W/(m^2 \cdot K)$)
P	power (W)

Subscripts

HTF	heat transfer fluid
$evap$	evaporator
$cond$	condenser
avg	average
i	inside surface/in
o	outside surface/out

</div>

Refs. [8]. Xia et al. [9,10] considered a series of enhanced heat transfer tubes featuring circumferential rectangular micro-grooves for experimental investigation. Refrigerant height inside the liquid pool, evaporation pressure, and degree of superheat were deemed influential. They also provided an analytical model in a later study [10]. Recently the use of CALPEs for larger scale evaporators, especially in adsorption cooling devices, have been reported in Ref. [11–17]. Thimmaiah et al. [12] studied the performance of a CALPE for SCS using water as the refrigerant and reported that the capillary-assisted tubes provide 1.6–2.2 times higher HTC compared to a plain tube with the same diameter. Similar data was published in Ref. [11]. Table 1 provides an overview of the experimental CALPE studies published in the literature.

As highlighted in Table 1, most studies focused only on CALPE. The focus of this study is to find out *whether a CALPE can be used as a condenser as well?* An efficient combined evaporator and condenser (CEC) with a comparable performance to that of separate evaporator and condenser can accelerate the development of a cost-effective and compact SCS.

In this paper four commercially available finned-tubes (supplied by Wolverine Tube Inc) are used to custom-build capillary-assisted heat exchangers with various fin geometries. The present CECs are tested under a wide range of operating conditions. The operating temperature range is chosen to reflect the real-life application of sorption systems. To our best knowledge, these enhanced tubes have not been studied for low pressure condensation before, therefore, their potential to be used as a CEC is studied for the first time in this study. Therefore, this study answers the following questions:

i) is a CEC a viable option for sorption cooling system? and,

ii) what are the cooling and heating capacities of the present CECs as a function of operating conditions?

2. Experimental study

Capillary-assisted heat exchangers were designed and built in-house, at the Laboratory for Alternative Energy Conversion [12], as shown in Fig. 1. Tests were conducted on four types of enhanced heat transfer tubes with various fin structures, as listed in Table 2.

Commercially available enhanced fin-tubes are limited. Especially small diameter tubes with high fin per inch (FPI) values are not widely manufactured. Small internal diameter is desirable to decrease the internal heat transfer resistance, as discussed at length in Ref. [12]. However, since the focus of this study is to investigate the performance of enhanced tubes as CEC, these four tubes were chosen regardless of their otherwise higher internal resistance (due to their ¾ inch diameter). A full discussion on total thermal resistance of CALPEs was given in Ref. [12]. All four CECs have a similar weight of ~870 g and take up ~420 cm^3 of space.

The heat exchangers had a four-pass arrangement (by copper welding, Fig. 1) with a total tube length of 1.54 m, tube diameter of 0.01905 m (3/4 inch), provided by Wolverine Tube Inc. As shown in Fig. 2, two temperature control systems (TCS, Julabo FP50-MA) provided a constant temperature heat transfer fluid (HTF, 50%–50% water and ethylene glycol mixture). Distilled water (1.35 L) was added to the evaporator chamber and was de-aerated prior to the experiments. Two vacuum chambers were connected with a short flexible hose and an electro-pneumatic gate valve (HVA KF50 with 12V solenoid valve).

The bigger chamber worked as a vapor generator or vapor

Table 1
Summary of published studies on capillary-assisted low-pressure evaporators (CALPE) — all with water as refrigerant and copper tubes.

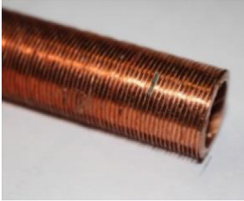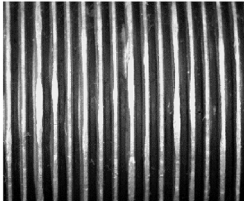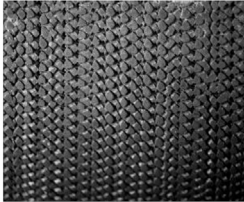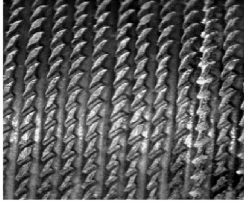|	Power (W)	P (kPa)	Coating	UA (W/K)	Notes
Thimmaiah et al. [12]	400	<1	coated/uncoated	46	Tested five different enhanced tubes and compared with plain tubes.
Lanzerath et al. [13]	600	1–2	coated/uncoated	56	Tested coated and uncoated plain and finned tubes.
Xia et al. [9]	450	~1	uncoated	63	Compared falling film to capillary assisted evaporators.
Sabir et al. [7]	1600	1.5	coated	—	Examined the effect of porous coating on capillary evaporation. Area not given but HTC of up to 5 kW/m^2 reported.
Schnabel et al. [15]	1200	1–2	uncoated	~100	Evaporation capacity of different tubes and flooding modes reported. UA value for LMTD of 3 K.
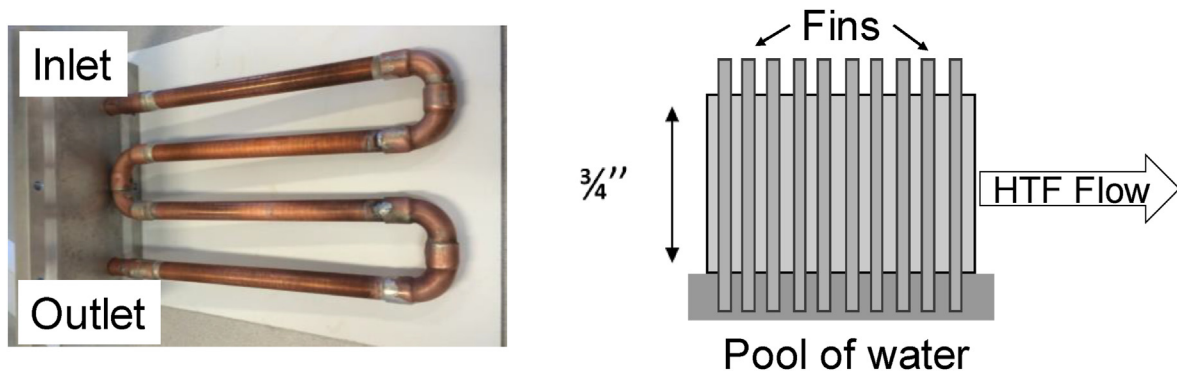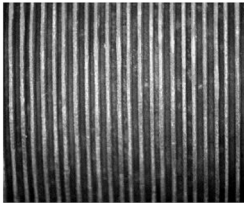
Fig. 1. Custom-built low-pressure heat exchanger used as combined evaporator and condenser (CEC). Internal tubes' diameter is ¾" — Left: four-pass, 1.54 m long evaporator made from Turbo Chil-26 FPI copper tube with parallel fins (supplied by Wolverine Tube Inc), Right: Schematic of a continuous fin capillary tube in evaporator mode.

Table 2
Geometry details of different enhanced tubes used in low pressure heat exchangers for CEC tests — test tubes are all made of copper and provided by Wolverine Tube Inc.

Name	Tube name and details	Fin structure	Zoomed view
CEC 1	Turbo Chil-26 FPI Fin Type: Continuous and parallel fins OD: 3/4" (19.05 mm) Fin Height: 1.422 mm Min. wall under fins: 0.737 mm Inside surface area: 0.049 m^2/m Outside surface area: 0.193 m^2/m		
CEC 2	Turbo Chil-40 FPI Fin Type: Continuous and parallel fins OD: 3/4" (19.05 mm) Fin Height: 1.473 mm Min. wall under fins: 0.635 mm Inside surface area: 0.051 m^2/m Outside surface area: 0.263 m^2/m		
CEC 3	Turbo ELP Fin Type: Interrupted micro pin fins OD: 3/4" (19.05 mm) Fin Height: 0.5 mm Min. wall under fins: 0.889 Inside surface area: 0.073 m^2/m Outside surface area: 194.8 m^2/m		
CEC 4	Turbo CLF-40 FPI Fin Type: Continuous with interrupted cross heads on top of the fin OD: 3/4" (19.05 mm) Fin Height: 0.965 mm Min. wall under fins: 0.787 mm Inside surface area: 0.0549 m^2/m Outside surface area: 0.2173 m^2/m		

collector. It was intentionally selected with a larger volume to prevent a bottleneck and not to affect the performance. The smaller chamber was used for testing of different heat exchangers, i.e., CEC. Prior to starting the experiments, two temperature control systems ran for at least an hour to ensure steady-state conditions. The temperature, pressure, and HTF flowrate in both chambers were monitored using seven RTD temperature sensors (OMEGA PT100), four pressure transducers with 0—34.5 kPa operating range (OMEGA PX309-005AI), and two flow meters (FLOMEC, Model # OM015S001-222). For evaporation tests, experiments were started with the heat exchanger in the smaller chamber submerged in water (flooded evaporator) and ended when the chamber was dry. For condensation tests, the smaller chamber with the heat exchanger was completely dried and vacuumed. Experiments started with opening of the gate valve between the two chambers. Operating pressure was the saturation pressure at the set temperature and ranged between 0.61 and 5.63 kPa for the tests. The flow rate was set to be 5.5 L per min (LPM) for both TCS. The aluminum
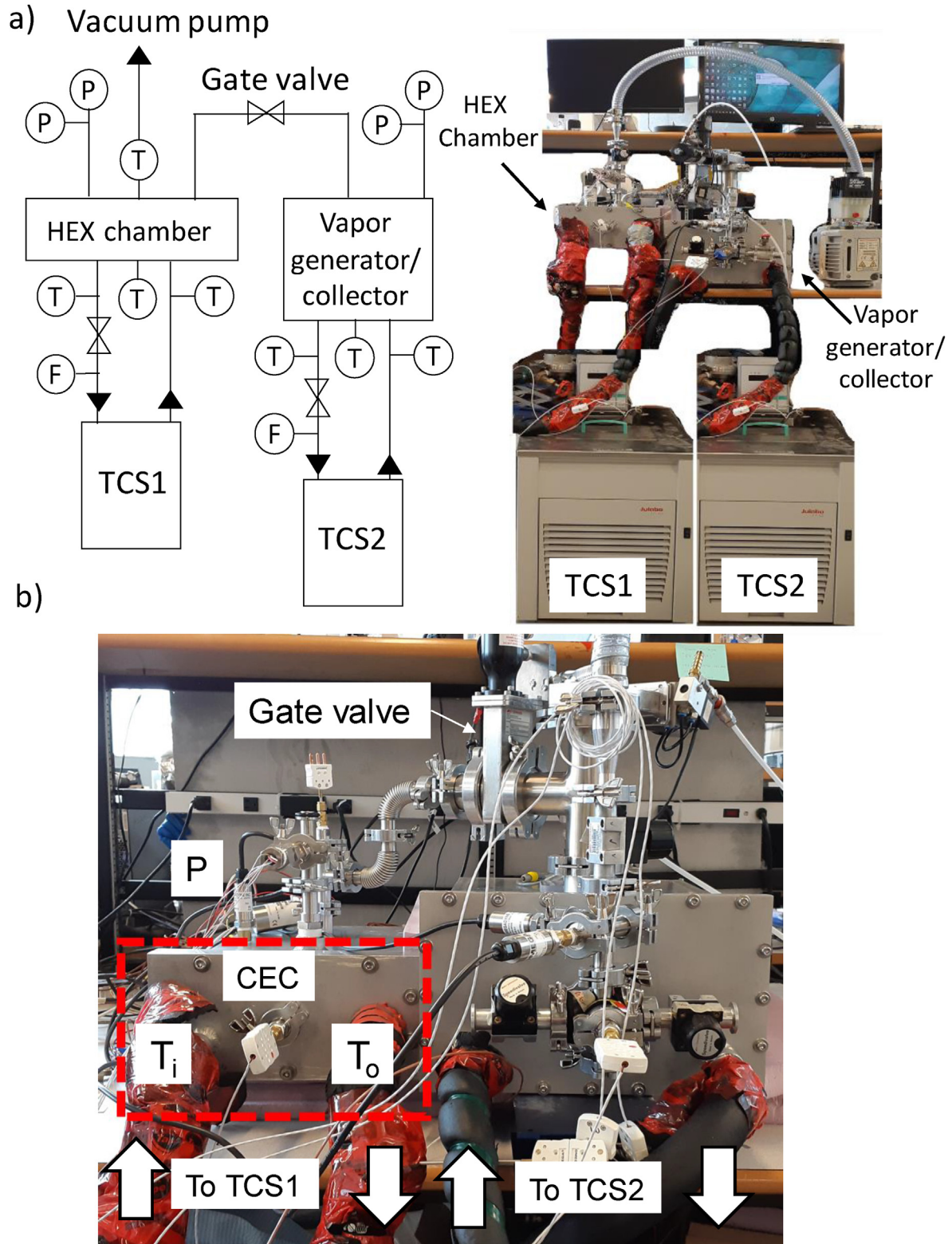
Fig. 2. Combined evaporator and condenser (CEC) test bed; a) Schematic of two-chamber test bed. A gate valve separates the two chambers, b) Photo of the test bed. P and T_i values are given in Table 3. The red box shows the smaller chamber where test heat exchangers were placed. (For interpretation of the references to colour in this figure legend, the reader is referred to the Web version of this article.)

vacuum chambers were triple coated with a protective polymer (ProtectaClear) to prevent corrosion (outgassing) and a 0.4 mm-thick Teflon sheet was inserted under the heat exchangers that

prevented direct contact between the copper heat exchanger and the chamber's aluminum walls (preventing galvanic corrosion). The smaller chamber was 0.343 m (13.5″) wide and 0.42 m (16.5″) long.

The operating conditions of this study are summarized in Table 3. All tests were performed with 1350 g of water and HTF flowrate of 5.5 LPM. The temperature of distilled water inside the vacuum chamber is not separately controlled by another heat exchanger and the water is let to evaporate by the CEC.

The temperature range was chosen to cover both evaporator and condenser operating conditions and spans from 0 to 35 °C. At each temperature, the heat exchanger's performance as both evaporator and condenser was evaluated and reported. The larger chamber's heat transfer fluid inlet temperature was maintained at a 5 °C difference with the smaller chamber. For example, when reporting the evaporator performance of a certain heat exchanger at 25 °C, the small chamber inlet temperature was set to 25 °C, and the larger chamber inlet temperature was set to 20 °C, maintaining a 5 °C temperature difference. When the same heat exchanger was evaluated as a condenser at 25 °C, the larger chamber worked as a vapor generator at 30 °C. This was adopted to enable a systematic comparison between the heat exchangers.

3. Uncertainty analysis

RTD temperature sensors with a ± 0.15 °C resolution were used in the measurement of HTF inlet and outlet temperatures. T-type thermocouples, accurate to ± 0.5 °C, were used to monitor temperatures inside the chamber. The pressure sensors were calibrated and had an accuracy of 0.08%. The flowmeter was accurate to $\pm 0.7\%$. Therefore, and considering the standard deviation of data measurement and sensor accuracy, the maximum uncertainty of the cooling and heating power was 9% [18].

4. Data analysis

The HTF inlet and outlet temperatures for both vacuum chambers were monitored and stored in an in-house LabView code. The calculations were based on the smaller chamber and its corresponding temperatures and flowrate. T_i and T_o denote the inlet and outlet temperature of HTF coming from the TCS, as shown in Fig. 2. More detailed operating conditions were given in Table 2.

The following relationship is used to calculate the heat flow rate [12,19]:

$$\dot{q} = \dot{m} c_p (T_i - T_o) \tag{1}$$

The total evaporation rate is then calculated by time averaging the heat flow rate over the steady-state period. By using Eq. (1):

$$\dot{Q} = \frac{\int_{t_1}^{t_2} \dot{q} dt}{\Delta t} \tag{2}$$

where, t_1 and t_2 are the beginning and end of the steady-state period, respectively. Finally, the overall heat transfer coefficient, UA (W/K), is:

$$UA = \frac{\dot{Q}}{\Delta T_{LMTD}} \tag{3}$$

Since different CECs have different heat transfer area, in order to

be consistent and have a better comparison, the overall heat transfer coefficient is reported as UA with unit of W/K.

The logarithmic mean temperature difference between the heat transfer fluid and the refrigerant is calculated by

$$\Delta T_{LMTD} = \frac{T_i - T_o}{\ln\left(\frac{T_i - T_{sat}}{T_o - T_{sat}}\right)} \tag{4}$$

T_{sat} is the average of the saturation temperature inside the chamber.

5. Results and discussion

The overall performance of a capillary tube CEC depends on the internal and external convective heat transfer coefficients as well as the heat conduction resistance in the tube wall. As previously mentioned, this paper only focuses on the CEC performance of the selected four enhanced tube without focusing on the internal film resistance, which is in fact the major bottleneck and can be reduced by reducing the tube diameters. Detailed discussion on the this topic can be found in Refs. [12]. Instead, here we present the feasibility of using the same evaporator as a condenser and provide a roadmap for capacity of existing tubes when they are used as CEC. Before we get to the results, we compare the output power and UA values of two chambers in Fig. 3. Fig. 3 (a) shows the evaporator power of CEC 4 as compared to condensation power of the vapor collector vs time and Fig. 3 (b) shows the UA values for evaporator power of CEC 4 as compared to UA of the vapor collector vs time. Both figures are for evaporation at 30 °C. In a non-capillary low-pressure evaporator, the only heat transfer mechanism is the natural (or forced, depending on the system) convection which has a direct relationship with the heat.

transfer area submerged in water. Therefore, in a non-capillary evaporator, the cooling power decreases with decreasing water height and the active heat transfer area. However, in a CALPE, the dominant heat transfer mechanism is the thin film evaporation which keeps the cooling power near constant even when the water height decreases [4,12]. Fig. 3 also makes a point in demonstrating negligible heat loss between the two chambers by using proper insulation and the fact that the two chambers' power outputs are almost identical.

Fig. 4 shows the measured evolution of cooling power for CEC 4 (see Table 2) over time. When the gate valve between the two chambers is opened, the evaporator pressure decreases, and then remains almost constant until the evaporator runs out of liquid water. Since the two TCS had been running prior to opening the valve, the inlet temperature showed a steady 30 °C. As mentioned previously, at the beginning of the experiment, the evaporator is flooded, thus the dominant heat transfer mechanism is natural convection due to the difference between the saturation temperature and the tubes' surface temperature [12]. As the water level decreases, the capillary effect starts, as the dominant mechanism, to affect the heat transfer and increases the cooling power significantly due to the addition of thin film evaporation, which is complemented by the natural convection heat transfer mechanism. Therefore, it is observed that a capillary tube is cable of maintaining an almost constant evaporation heat transfer rate and outlet temperature of HTF for a desired period of time. The hydrostatic pressure causes a pressure difference between liquid-vapor interface and the bottom of the evaporator. Consequently, saturation temperature of liquid increases at the bottom, leading to decrease in temperature difference between the HTF and the liquid water outside, reducing the cooling power. The hydrostatic pressure reduces as the evaporation lowers the water level and the heat

Table 3
Operating conditions for the experiments – All tests performed with 1350 g of water and HTF flowrate of 5.5 LPM.

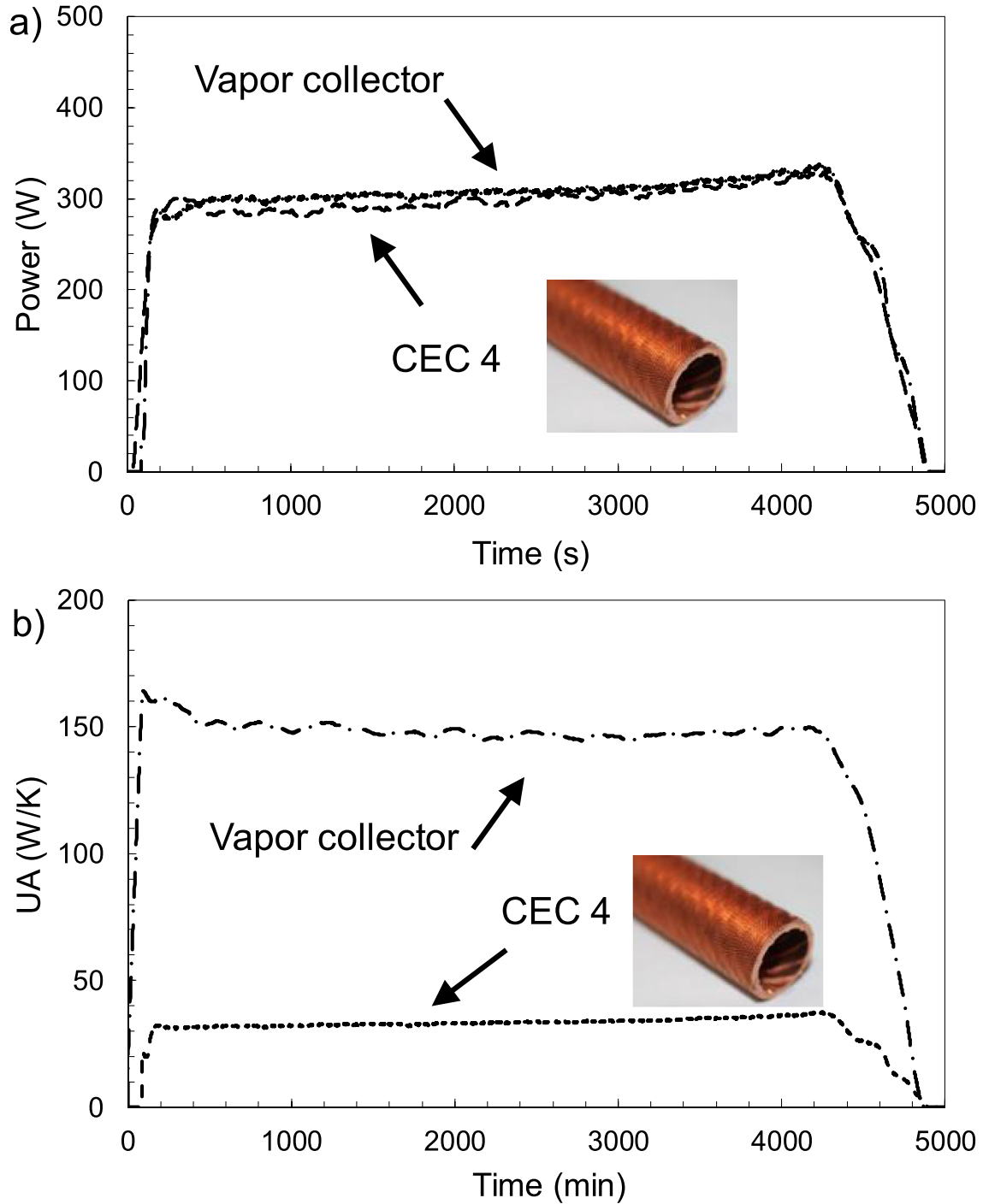| Parameter	Values							
Inlet temperature, T_i (°C)	0	5	10	15	20	25	30	35
Chamber pressure, P (kPa)	0.61	0.87	1.23	1.7	2.34	3.17	4.24	5.63

Fig. 3. a) Evaporator power of CEC 4 as compared to condensation power of the vapor collector vs time, b) UA values for evaporator power of CEC 4 as compared to UA of the vapor collector vs time − (see Table 2 for CEC specifications) − operating conditions: small chamber HTF inlet temperature at 30 °C, big chamber HTF inlet temperature 25 °C, average evaporator pressure of 4.24 kPa, and HTF flowrate of 5.5 LPM.

transfer rate increases. The heat transfer rate remains high as the water level decreases further due to thin film capillary evaporation.

This trend continues until the evaporator is dry. As shown in Fig. 4 the HTF outlet temperature drops accordingly and maintains at a somewhat constant 2 °C temperature difference with HTF inlet over the steady state period. The evaporator runs out of water at the end and the dry-out period starts until it completely runs out of water at the end of the test.

The internal heat transfer coefficient can be calculated by following expression [21]:

$$\frac{1}{UA} = \left(\frac{1}{h_o A_o} + \frac{1}{h_i A_i} + R_{o,\ finned\ tube} \right) \quad (5)$$

The first term on the right hand side of the Eq. (5) describes the external convective heat resistance due to capillary evaporation, the second term is the internal convective heat resistance due to
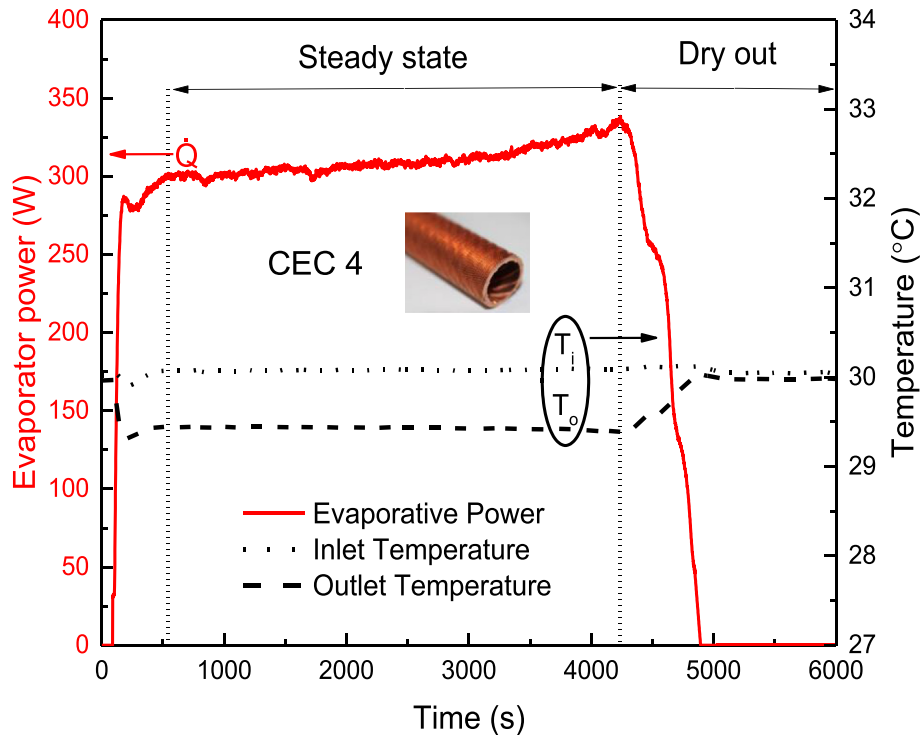
Fig. 4. Evaporator power and HTF inlet and outlet temperature for CEC 4 — operating conditions: small chamber HTF inlet temperature at 30 °C, big chamber HTF inlet temperature 25 °C (not shown), average evaporator pressure of 4.24 kPa, and HTF flowrate of 5.5 LPM. Steady state period is demarcated.

single phase flow inside the tube, and the third term is the conductive heat resistance of the tube wall. Table 4 summarizes the overall thermal resistance of CEC 4 based on the obtained results in Fig. 3; namely, UA = 33 W/K. Therefore, the total thermal resistance would be 0.0303 K/W. Given that the wall resistance is 6×10^{-4} and the internal resistance of the HTF equals 1×10^{-2} K/W, then the external resistance for the film evaporation is estimated to 1.97×10^{-2} K/W. This implies that $h_o A_o = 50.75$ W/K. Given the external surface area is 1.54×0.217 m^2, the external heat transfer coefficient for the film evaporation, h_o, can be estimated to be 151.66 W/m$^2 \cdot$K, based on the tubes outside surface area, at 30 °C inlet temperature.

In Fig. 5, the performance of CEC 4 as a condenser is shown. At the beginning of the experiment, CEC 4 is dry, thus it shows the highest condensation power. When water starts to accumulate on the surface of the tubes, its performance drops but still remains high for almost 4 min. As an evaporator, CEC 4 was able to maintain a high performance for at least twice that time. In fact, since the heat exchanger in the big chamber is intentionally chosen to be larger, the condenser does not run out of water vapor, therefore, the decrease in the condenser power is due to its inability to keep up with the incoming amount of water vapor.

HTF inlet and outlet temperatures are also presented to show the corresponding trends. Nevertheless, it can be concluded that a capillary tube performs well as both evaporator and condenser. It should be noted that this paper only deals with steady state results and does not take into account the effect of unsteady temperature jumps. Under a more realistic condition, the effect of temperature

swinging from condensation to evaporation temperature should also be studied. In such dynamic tests, the thermal inertia of a CEC will be a key parameter and should be considered. The transient data for the rest of the CECs are not presented for brevity.

Fig. 6 summarizes the evaporator performance results for all CECs listed in Table 2. In each case, as mentioned, there is a 5 °C temperature difference between the two vacuum chambers. The evaporator power and their associated overall heat transfer coefficient are calculated from the steady state period data and presented. It is observed that the evaporator power of CECs is more or less similar. CEC 2 with parallel continuous fins performs better as an evaporator followed by CEC 3, which is originally designed to be an evaporator. Correlations based on curve-fitting of the data are provided for each CEC and each test mode. The average UA values are curve-fitted by the equations given in Figs. 6 and 7. These correlations predict the average UA of each CEC, at a given evaporator and condenser temperature rather accurately.

Fig. 7 compares the condenser performance of the four enhanced tube CECs. A similar trend to those presented in Fig. 6 is observed. Expectedly, CEC 4 has the poorest performance as an evaporator and the best performance as a condenser, since it is designed to work as a condenser. Comparing the evaporator and condenser performance of the studied CECs, as shown in Figs. 6 and 7, indicates that having continuous parallel fins, higher fin heights, and high heat transfer surface area, as in Turbo Chil-40 FPI, leads to a better combined evaporator and condenser [17] since they offer lower thermal resistance. As a result, it can be concluded that the evaporator built with Turbo Chil-40 FPI, CEC 2, for SCS can be used

Table 4
Conductive and Convective resistances for CEC 4 with copper with thermal conductivity of 340 W/m.K

External resistance (K/W)	Wall resistance (K/W)	Internal resistance (K/W)	Overall thermal resistance (K/W)
1.97×10^{-2}	6×10^{-4}	1×10^{-2}	3.03×10^{-2}

Table 5
Correlations based on curve-fitting of the data for each CEC and each test mode.

Evaporator UA		
CEC 1	$UA_{avg} = 26.01 + 0.21\, T_{evap} + 0.009\, T_{evap}^2$	Eq. (6)
CEC 2	$UA_{avg} = 30.01 + 0.13\, T_{evap} + 0.003\, T_{evap}^2$	Eq. (7)
CEC 3	$UA_{avg} = 25.10 + 0.05\, T_{evap} + 0.005\, T_{evap}^2$	Eq. (8)
CEC 4	$UA_{avg} = 23.63 - 0.15\, T_{evap} + 0.014\, T_{evap}^2$	Eq. (9)
Condenser UA		
CEC 1	$UA_{avg} = 43.02 - 0.03\, T_{cond} - 0.004\, T_{cond}^2$	Eq. (10)
CEC 2	$UA_{avg} = 42.82 - 0.11\, T_{cond} - 0.005\, T_{cond}^2$	Eq. (11)
CEC 3	$UA_{avg} = 44.23 + 0.08\, T_{cond} - 0.012\, T_{cond}^2$	Eq. (12)
CEC 4	$UA_{avg} = 46.43 - 0.18\, T_{cond} - 0.002\, T_{cond}^2$	Eq. (13)

as an efficient CEC, leading to a compact modular design.

A direct comparison with many published data in the literature is almost impossible due to the difference in operating conditions, tube size, and experimental set ups. Nevertheless, a comparison is made in Fig. 8 with data from Ref. [12] where a vacuum pump was used instead of a vapor collector. It is seen that although the data are very similar, using a vacuum pump instead of a vapor collector has a slight improvement since the water vapor is immediately removed and there is no condensation process potentially limiting the evaporation. The effect of different experimental setups can be read in Ref. [20]. The x-axis is chosen to be the pressure difference between the evaporator chamber and the collector chamber. The latter would be zero for the setup with the vacuum pump [12].

6. Conclusions

Four types of capillary-assisted tubes were considered for a low-pressure CEC application in SCS. The heat exchangers were tested at the pressure range of 0.61−5.63 kPa with working fluid inlet temperatures ranging from 0 to 35 °C. The total heat transfer rate and

overall heat transfer coefficient for evaporation and condensation phases were experimentally investigated and reported. For the first time, the potential of using commercially available enhanced tubes for a combined low pressure evaporator and condenser was tested. Two questions regarding i) the feasibility, and ii) capacity of CECs were answered in this paper. It was also observed that:

- Tubes with 1.42 mm parallel fins (40 fins per inch (FPI)) had a higher HTC as an evaporator (40 W/K)
- Tubes with 0.9 mm cross head fins (40 FPI) marginally outperformed other tubes as a condenser (47 W/K).
- The Turbo Chil-40 FPI provided the best combination of evaporation and condensation performance.

Following the evaluation of low-pressure evaporators and condensers, the CEC with the better combined performance (Turbo Chil-40 FPI) is currently being used in tests of a lab-scale modular SCS system. A low-pressure CEC with significantly small HTF internal tube (or hydraulic) diameters is being optimized to reduce the thermal inertia and the amount of HTF inside the heat exchanger.

Credit author statement

All authors have contributed to this work equally.

Declaration of Competing Interest

The authors declare that they have no known competing financial interests or personal relationships that could have appeared to influence the work reported in this paper.
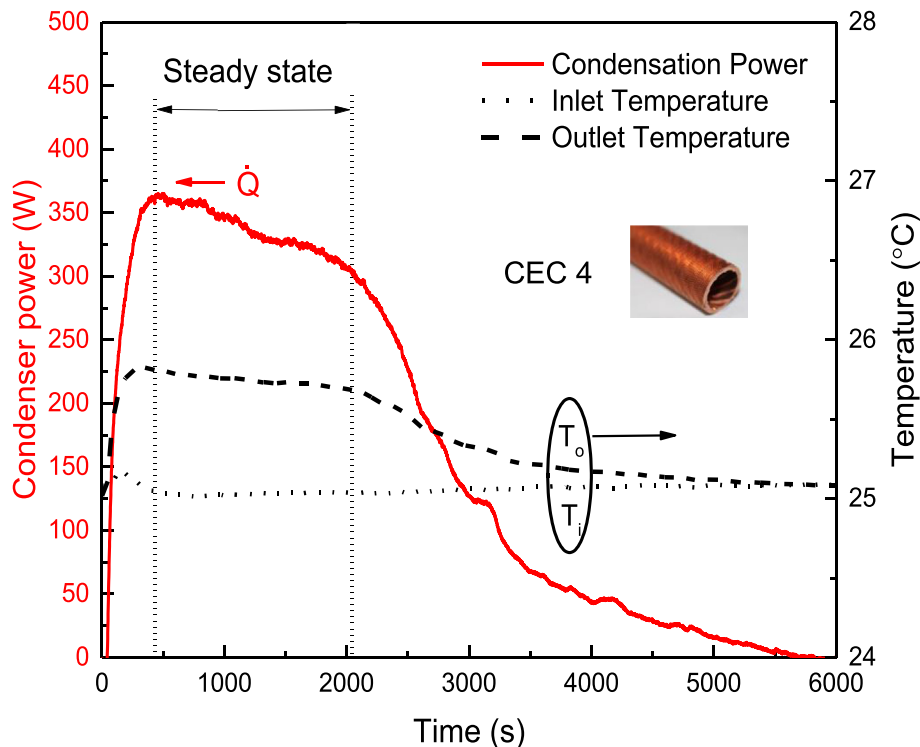

Fig. 5. Condenser power and HTF inlet and outlet temperature for CEC 4 − operating conditions: small chamber HTF inlet temperature at 25 °C, big chamber HTF inlet temperature 30 °C (not shown), average condenser pressure of 3.17 kPa, and HTF flowrate of 5.5 LPM. Steady state period is demarcated.
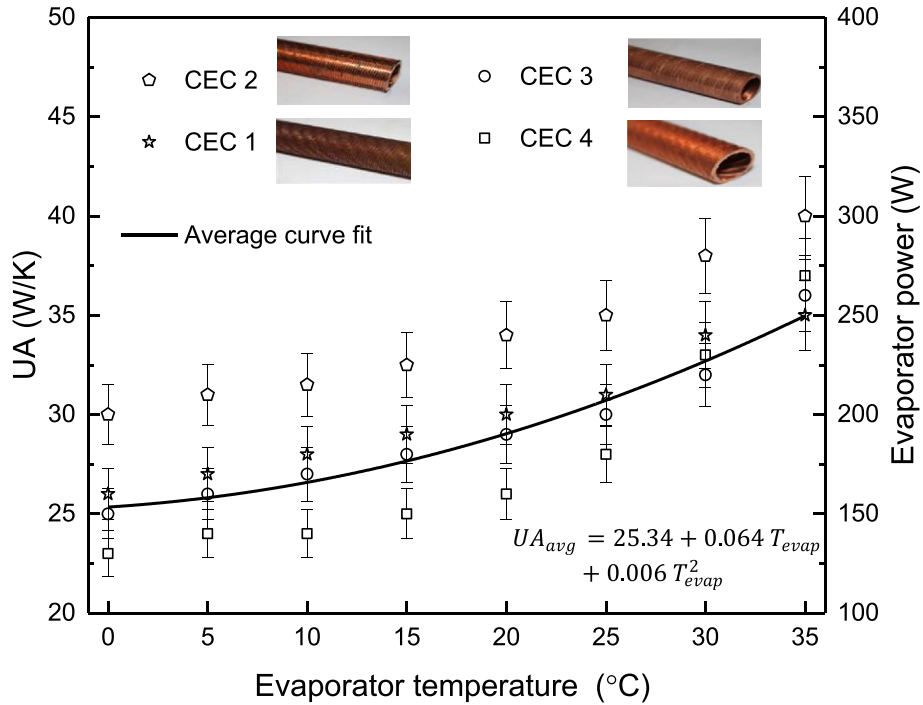
Fig. 6. UA and evaporator power vs evaporation temperature (HTF inlet temperature) for four CECs. (see Table 2 for CEC specifications). Evaporation test conditions: small chamber HTF inlet temperature ranging from 0 to 35 °C, HTF flowrate at 5.5 LPM, evaporator pressure ranging from 0.61 to 5.63 kPa. A curve fit function is also presented to predict average UA of four CECs at a given evaporation temperature. Correlations for all CECs can be found in Table 5.
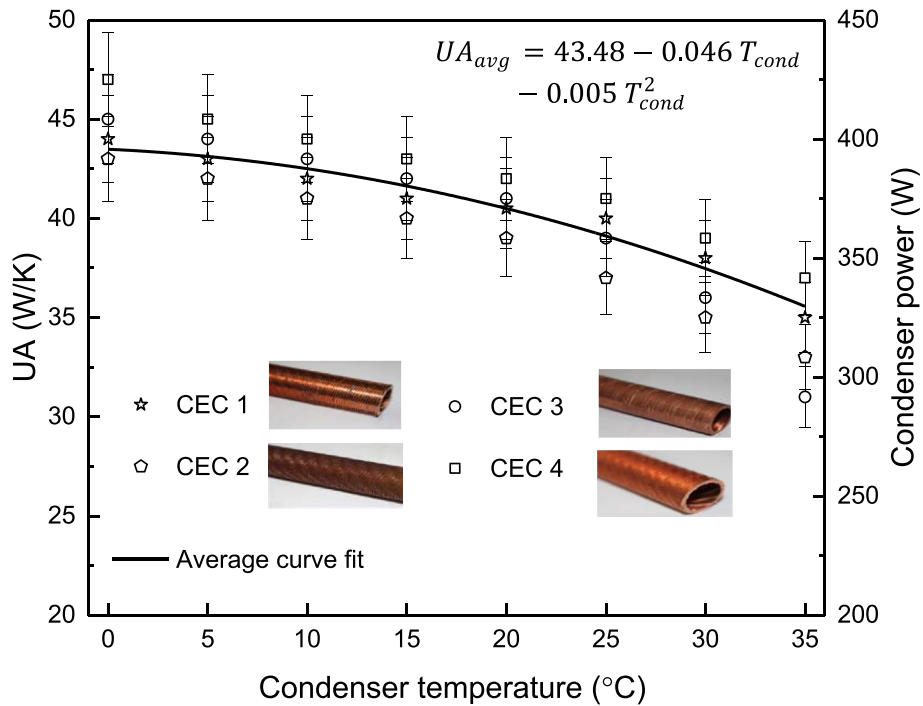
In Fig. 6:
$$UA_{avg} = 25.34 + 0.064\,T_{evap} + 0.006\,T_{evap}^2$$

Fig. 7. UA and condenser power vs condensation temperature (HTF inlet temperature) for four CECs. (see Table 2 for CEC specifications). Condensation test conditions: small chamber HTF inlet temperature ranging from 0 to 35 °C, HTF flowrate at 5.5 LPM, condenser pressure ranging from 0.61 to 5.63 kPa. A curve fit function is also presented to predict average UA of four CECs at a given condensation temperature. Correlations for all CECs can be found in Table 5.
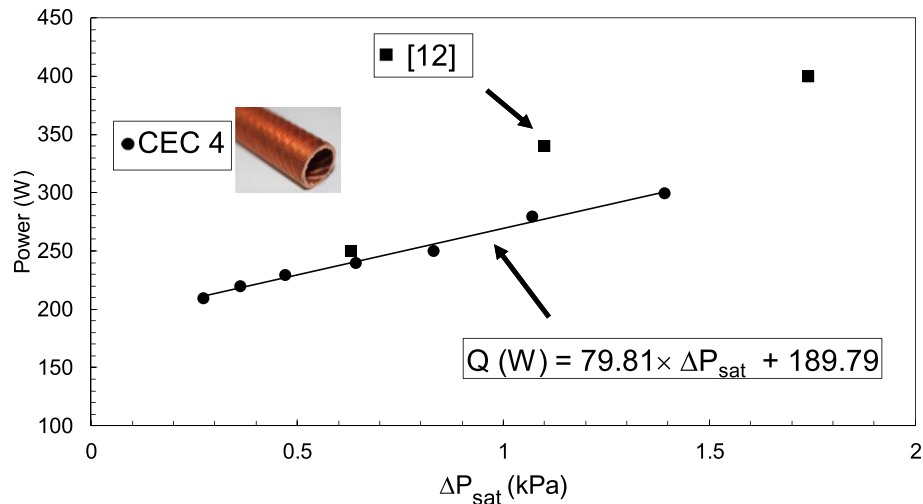
In Fig. 7:
$$UA_{avg} = 43.48 - 0.046\,T_{cond} - 0.005\,T_{cond}^2$$

G.B. Abadi, M. Bahrami / Energy 209 (2020) 118504

Fig. 8. A comparison with data from Ref. [12] where a vacuum pump was used instead of a vapor collector. The x-axis is the saturation pressure difference between the evaporator chamber and the collector chamber. Average values are used for comparison.

References

[1] U.S. Department of Energy. Buildings energy databook. Energy Effic Renew Energy Dep; 2012. p. 286.

[2] Askalany AA, Salem M, Ismael IM, Ali AHH, Morsy MG, Saha BB. An overview on adsorption pairs for cooling. Renew Sustain Energy Rev 2013;19:565—72. https://doi.org/10.1016/j.rser.2012.11.037.

[3] Pridasawas W. Solar-driven refrigeration systems with focus on the ejector cycle. 2006. https://doi.org/10.1677/joe.0.1270351.

[4] Thimmaiah PC, Sharafian A, Rouhani M, Huttema W, Bahrami M. Evaluation of low-pressure flooded evaporator performance for adsorption chillers. Energy 2017;122:144—58. https://doi.org/10.1016/j.energy.2017.01.085.

[5] Wang RZ, Oliveira RG. Adsorption refrigeration-An efficient way to make good use of waste heat and solar energy. Prog Energy Combust Sci 2006;32: 424—58. https://doi.org/10.1016/j.pecs.2006.01.002.

[6] Lemmon EW, Bell IH, Huber ML, McLinden MO. NIST standard Reference Database 23: Reference fluid Thermodynamic and Transport Properties-REFPROP. National Institute of Standards and Technology; 2018. p. 135. https://doi.org/10.18434/T4JS3C. Version 9.0.

[7] Sabir HM, ElHag YBM, Benhadj-Djilali R. Experimental study of capillary-assisted evaporators. Energy Build 2008;40:399—407. https://doi.org/10.1016/j.enbuild.2007.02.036.

[8] Sabir HM, ElHag YBM. A study of capillary-assisted evaporators. Appl Therm Eng 2007;27:1555—64. https://doi.org/10.1016/j.applthermaleng.2006.09.011.

[9] Xia ZZ, Yang GZ, Wang RZ. Experimental investigation of capillary-assisted evaporation on the outside surface of horizontal tubes. Int J Heat Mass Tran 2008;51:4047—54. https://doi.org/10.1016/j.ijheatmasstransfer.2007.11.042.

[10] Xia ZZ, Yang GZ, Wang RZ. Capillary-assisted flow and evaporation inside circumferential rectangular micro groove. Int J Heat Mass Tran 2009;52: 952—61. https://doi.org/10.1016/j.ijheatmasstransfer.2008.05.041.

[11] Cheppudira Thimmaiah P, Sharafian A, Huttema W, Osterman C, Ismail A, Dhillon A, et al. Performance of finned tubes used in low-pressure capillary-assisted evaporator of adsorption cooling system. Appl Therm Eng 2016;106: 371—80. https://doi.org/10.1016/j.applthermaleng.2016.06.038.

[12] Cheppudira Thimmaiah P, Sharafian A, Huttema W, McCague C, Bahrami M. Effects of capillary-assisted tubes with different fin geometries on the performance of a low-operating pressure evaporator for adsorption cooling system applications. Appl Energy 2016;171:256—65. https://doi.org/10.1016/j.apenergy.2016.03.070.

[13] Lanzerath F, Seiler J, Erdogan M, Schreiber H, Steinhilber M, Bardow A. The impact of filling level resolved: capillary-assisted evaporation of water for adsorption heat pumps. Appl Therm Eng 2016;102:513—9. https://doi.org/10.1016/j.applthermaleng.2016.03.052.

[14] Sabir HM, Bwalya AC. Experimental study of capillary-assisted water evaporators for vapour-absorption systems. Appl Energy 2002;71:45—57. https://doi.org/10.1016/S0306-2619(01)00042-3.

[15] Schnabel L, Witte K, Kowol JSP. Evaluation of different evaporator concepts for Thermally driven sorption Heat Pumps and Chiller. Int Sorption Heat Pump Conf 2011:525—43. https://doi.org/10.1081/E-EEE2-120046011.

[16] Cheng P, Dong J, Thompson SM, Ma HB. Heat transfer in bulk and thin-film fluid regions of rectangular microgroove. J Thermophys Heat Tran 2012;26: 108—14. https://doi.org/10.2514/1.T3684.

[17] Thimmaiah PC. Development of capillary - assisted low pressure evaporator for adsorption chillers. PhD Thesis 2016;1—56.

[18] Holman JP. Experimental methods for Engineers, s1-VIII; 1853. https://doi.org/10.1093/nq/s1-VIII.193.43-b.

[19] J.P. H. Heat transfer. 2008. https://doi.org/10.1016/b978-1-933762-24-1.50019-x.

[20] J. Seiler, Rahel volmer, dennis krakau, julien pöhls, franziska ossenkopp, lena schnabel, andré bardow, capillary-assisted evaporation of water from finned tubes — impacts of experimental setups and dynamics, Appl Therm Eng Volume 165, 25 January 2020, 114620.

[21] Bergman Theodore L, Lavine Adrienne S, Frank P, Incropera DPD. One-dimensional, steady-state conduction, Fundamenta. John WIiley & Sons, Inc; 2014. https://doi.org/10.1007/s13398-014-0173-7.2.